Journal of Asian Earth Sciences 148 (2017) 315–323

Contents lists available at ScienceDirect

Journal of Asian Earth Sciences

journal homepage: www.elsevier.com/locate/jseaes

Full length Article

Some IR features of SiO_4 and OH in coesite, and its amorphization and dehydration at ambient pressure

Xi Liu[a,b,*], Yunlu Ma[a,b], Qiang He[c], Mingyue He[d,*]

[a] The Key Laboratory of Orogenic Belts and Crustal Evolution, Ministry of Education of China, Beijing 100871, China
[b] School of Earth and Space Sciences, Peking University, Beijing 100871, China
[c] Institute of Fluid Physics, China Academy of Engineering Physics, Mianyang 659000, China
[d] School of Gemmology, China University of Geosciences (Beijing), Beijing 100083, China

ARTICLE INFO

Keywords:
Coesite
IR features
Water content
Dehydration
Subduction zone fluid
Amorphization

ABSTRACT

Coesite (Coe) with grain size in the range of 30–80 μm has been synthesized at 5 GPa and 1600 °C for 12 h by using a cubic press. Its unpolarized single-crystal absorption infrared (IR) spectra show 14 IR bands in the range of ~1200–650 cm^{-1}, five of which have high intensity (at ~1161, 1109, 1063, 1028 and 994 cm^{-1}) and are preliminarily assigned to the SiO_4 asymmetric stretching (ν_3). In addition, three sharp but relatively weak bands at ~838, 814 and 796 cm^{-1} are tentatively attributed to the SiO_4 asymmetric bending (ν_4). The IR data also show six OH peaks in the range of 3700–3300 cm^{-1}, with an estimated H_2O content of ~30(4) wt ppm. Following previous studies, we have assigned the peaks at ~3464 (#7), 3421 (#8), 3406 (#9) and 3377 cm^{-1} (#10) to the Type-II hydrogarnet substitution, and the peaks at ~3500 (#6a) and 3534 cm^{-1} (#6b) to the B-based defects, with the latter aroused by possible B contamination in the synthesizing experiments. Annealing experiments conducted consecutively at ~200, 400, 600, 800, 1000 and 1200 °C, with every heating step lasting for 24 h, demonstrate that water diffuses quickly out of Coe at *T* as low as ~600 °C. The material annealed at 1200 °C is completely dehydrated and amorphous. A quick response of the water content in Coe to the changes of *P*, *T* and composition is thus possible, which may be critical to the preservation of natural Coe in relevant geological processes. It further implies that water in Coe, and possibly in other nominally anhydrous minerals (NAMs), may behave distinctively different from the water located in the hydrous phases such as amphibole and mica, and potentially makes significant contribution to the subduction zone-related fluids.

1. Introduction

Coesite (Coe) was first synthesized in high-*P* laboratory (Coes, 1953) and later found in the sandstone at Meteor Crater, Arizona (Chao et al., 1960). Since its discovery in the regional metamorphic rocks of the Dora-Maira massif in the Western Alps (Chopin, 1984), it has attracted substantial attention in the geological community, simply because it indicates for the continental crust a deep subduction to depths of ~100 km or more with a subsequent fast returning to the surface of the Earth. A lot of effort has been devoted to investigate its crystal structure (e.g. Araki and Zoltai, 1969; Smyth et al., 1987; Geisinger et al., 1987), its physical properties such as the expansivity (e.g. Skinner, 1962; Bourova et al., 2006), the compressibility (e.g. Levien and Prewitt, 1981; Angel et al., 2001, 2003; Chen et al., 2016) and the sound velocity (e.g. Chen et al., 2015), its phase stability and phase relationship (e.g. Akaogi et al., 1995; Atake et al., 2000; Černok et al., 2014; Chen et al., 2016), its vibrational property (e.g. Lyon, 1962; Boyer et al., 1985; Hemley, 1987; Williams et al., 1993), its water solubility and water-incorporation mechanism (e.g. Mosenfelder, 2000; Koch-Müller et al., 2001, 2003; Thomas et al., 2009; Deon et al., 2009), and etc. The knowledge obtained on Coe has significantly deepened our understanding of the relevant geological systems and their processes at corresponding high *P*-high *T* conditions.

There are still some poorly-understood but important aspects of Coe remaining to be explored though. One of them is the infrared (IR) spectral data which are presently incomplete and in controversy (Dowty, 1987; Della Valle and Andersen, 1991; Koike et al., 2013). All existing experimental investigations (Lippincott et al., 1958; Austin et al., 1961; Lyon, 1962; Kieffer, 1979a; Williams et al., 1993; Koike et al., 2013) obtained powder IR spectra only, which might bear large uncertainties in the peak positions and intensities due to coupling of vibration frequencies and some particularities such as the effects of

* Corresponding authors at: School of Earth and Space Sciences, Peking University, Beijing 100871, China (X. Liu); School of Gemmology, China University of Geosciences (Beijing), Beijing 100083, China (M. He).
E-mail addresses: xi.liu@pku.edu.cn (X. Liu), hemy@cugb.edu.cn (M. He).

http://dx.doi.org/10.1016/j.jseaes.2017.03.016
Received 13 February 2017; Received in revised form 16 March 2017; Accepted 17 March 2017
Available online 18 March 2017

grain size and particle shape unavoidable in the sample preparation (Beran et al., 2004). Indeed, the experimental observation and the calculated IR spectrum of Coe are too different, as shown in Dowty (1987; Fig. 7). Considering the importance of such vibrational data in understanding or calculating the thermodynamic properties such as heat capacity and entropy (Kieffer, 1979b), IR data from Coe single crystals are highly desirable.

Another aspect is about the water enigma: synthetic Coe may contain up to 200 wt ppm water whereas natural Coe has been found as nearly dry (usually < 1 wt ppm; Rossman and Smyth, 1990; Mosenfelder, 1997). As the kinetics studies of the Coe → quartz phase transition attribute an accelerating effect to the structurally-bound OH in Coe on this phase transition (Mosenfelder and Bohlen, 1997; Lathe et al., 2005), the water-incorporation mechanism, the water solubility and its correlation to *P*, *T* and composition, and the dehydration process may set important constraints on the preservation of Coe in natural rocks (Mosenfelder et al., 2005). So far some experimental studies have been conducted to explore the water-incorporation mechanism in Coe and to constrain the water solubility (Mosenfelder, 2000; Koch-Müller et al., 2001, 2003; Thomas et al., 2009; Deon et al., 2009). But in order to unveil the water enigma of Coe, more experiments are required, particularly in the research fields of water diffusion and dehydration.

In this study, we synthesized Coe of large grain size using a cubic press, probed its single-crystal absorption IR features with special attention paid to those caused by the SiO_4 and OH, explored its dehydration process via annealing the sample at different *T*. At the same time, the amorphization process of Coe at ambient *P* was also investigated.

2. Experimental methods

Our Coe samples were synthesized at 5 GPa and 1600 °C by using the CS-IV 6 × 14 MN cubic press at the High-Pressure Laboratory of Peking University (Liu et al., 2012), and with the new cell arrangement reported in He et al. (2014; named as BJC-11 hereafter). The experimental pressure was calibrated at ambient *T* by using the high-*P* phase transitions of Bi (I–II transition at 2.55 GPa, and II–III transition at 2.69 GPa) and Ba (I–II transition at 5.5 GPa). The experimental temperature was measured and controlled by using a $Pt_{94}Rh_6$-$Pt_{70}Rh_{30}$ thermocouple, with any potential pressure effect on the e.m.f. ignored. The starting material (analytical grade SiO_2 powder from Alfa Aesar) for the high-*P* synthesizing experiments was pretreated at 1 atm and 300 °C for 72 h, subsequently loaded into Pt capsules (2 mm in diameter and ~5 mm in length), and heated for 12 h at the designed *P-T* conditions.

The experimental products were processed and examined by an optical microscope, a scanning electron microscope (Quanta 650 FEG), a confocal micro-Raman system (Renishaw system RM-1000) and an electron microprobe (JEOL JXA-8100), and confirmed to be pure polycrystalline Coe with grain sizes ranging from ~30 to 80 μm.

To make the free-standing, doubly polished thin sections for the transmission FTIR analysis, the general preparing procedures outlined in Liu et al. (2006) were followed. The high-*P* experimental products were sliced with a diamond saw, mounted on glass slides with crystal-bond and manually ground under water with a series of silicon carbide abrasive films. Four thin sections were successfully made, with their thicknesses measured by a micrometer as 60, 19, 15 and 10 μm; the accuracy in the thickness measurement was probably in the range of 2 μm (Liu et al., 2006). The thin sections less than 20 μm thick were slightly wedged, and readily broke down to loose crystal plates when washed under acetone. Nevertheless, a few crystal plates from each of these three thin sections were picked up under an optical microscope, transferred and placed on a BaF_2 sample holder, and analyzed by the FTIR (Fig. 1).

Transmission IR spectra were recorded with a Nicolet iN10 MX IR Microscope, newly installed at the High-Pressure Laboratory of Peking University (Tang et al., 2014; Wang et al., 2015). We used a high-energy Ever-Glo™ infrared source, a standard KBr beam splitter, and an MCT detector which was cooled by liquid N_2 to achieve an exceptional sensitivity down to ~10 μm. No polarizer was employed in this study. An aperture size of 40 × 40, 30 × 30 or 20 × 20 μm^2 was chosen for our FTIR analysis, depending on the size of the bright and clear light pathway of the Coe grains. We performed either 256 or 512 scans in every individual analysis, both for the background and for the sample (with the background analyzed first).

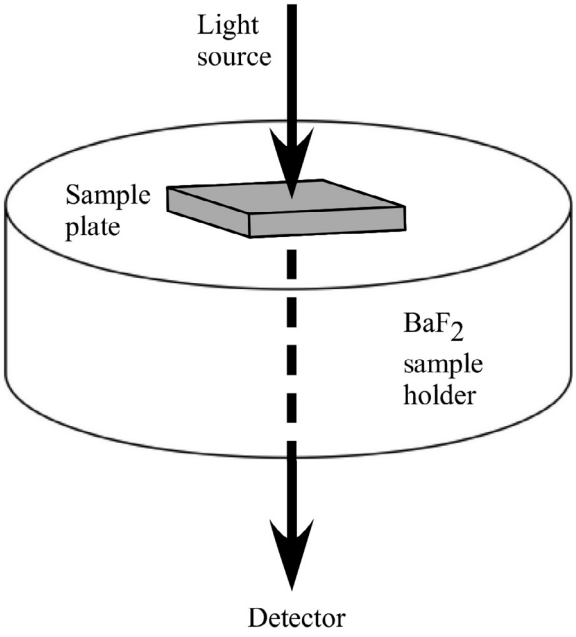

Fig. 1. Schematic setting-up in the transmission IR experiments. The unpolarized incident light from the high-energy Ever-Glo™ infrared source normally traveled through the sample plate and the BaF_2 sample holder, and entered the liquid N_2-cooled MCT detector. The doubly-polished and free-standing sample plate was either a single-crystal plate, or a multiple-crystal plate which contained a number of big crystals with bright and clear light pathway. The BaF_2 sample holder is transparent for the IR light at least in the energy range of ~4000–600 cm^{-1}. In this study, we probed single crystals of Coe only, and the IR data should be "pure" and 100% arise from the transverse optic modes (without any influence of the longitudinal optic modes). For the same sample, any real difference in the IR data collected from different crystals must originate from the difference in the crystal thickness and crystallographic orientation.

The annealing experiments at ambient *P* were conducted by using a high-*T* furnace at 200, 400, 600, 800, 1000 and 1200 °C, with no particular attention paid to the experimental *T* which therefore might be subject to an uncertainty as large as 10°. The sample used in these experiments was the 60-μm-thick FTIR thin section. Due to the large thickness of this sample compared to the Coe grain size (~30 to 80 μm), only a few Coe crystals with bright and clear light pathway could be found, so that they were generally traced and analyzed by the FTIR. After finishing one round of FTIR analyses, it was placed on a Pt disc, annealed for 24 h at a target *T* (with a heating-up and cooling-down ramp of 4 and −4 °C/min, respectively), and subsequently analyzed again with the FTIR.

3. Result and discussion

3.1. IR features of SiO_4 tetrahedron in Coe

Coe is a monoclinic mineral, and the irreducible representation of its optical vibrations can be expressed as (Hemley, 1987):

$$\Gamma_{op} = 16A_g + 17B_g + 18A_u + 18B_u,$$

with the A_g and B_g modes Raman-active and the A_u and B_u modes IR-active. So far at most 22 infrared bands have been experimentally

Table 1
IR frequencies (cm^{-1}) of Coe at ambient conditions.[a]

W2013	L1958	L1962	K1979	W1993	K2013	TS1	TS2
1295(w)[b]	–[c]	–	–	–	–	–	–
1285(vw)	–	–	–	–	–	–	–
1213(w)	1225	1218	1229	1225	–	–	–
1204(w)	–	–	–	–	–	1199(w)	–
1152(s)	1170	1152	1155	1170	–	1161(s)	–
1132(w)	–	–	–	–	–	–	–
1125(vs)	1098	1077	1100	1097	–	1109(vs)	–
1092(vs)	–	–	–	–	1091	1063(vs)	–
–	1040	1036	1040	1040	–	1028(vs)	–
–	–	–	–	–	–	994(s)	–
–	–	–	(960?)	–	–	965(w)	960(vw)
–	–	–	–	–	–	940(vw; ?)	944(vw)
872(vw)	–	–	(880?)	–	–	898(w)	901(w)
847(w)	–	837	(840?)	–	–	–	838(w)
827(w)	813	814	(811?)	814	813	–	814(s)
–	796	794	792	795	794	–	796(w)
703(w)	–	–	–	–	–	720(vw; ?)	719(vw)
692(vw)	683	683	681	683	685	686(w)	–
612(w)	**598**	**600**	**599**	**600**	**602**	–	–
561(w)	**557**	**561**	**561**	**557**	**562**	–	–
495(w)	–	**490**	**(490?)**	**490**	–	–	–
457(w)	–	–	–	–	–	–	–
444(w)	**442**	**448**	**448**	–	**444**	–	–
421(w)	–	–	438	–	–	–	–
420(w)	**430**	**435**	**420**	**430**	**422**	–	–
394(w)	**390**	–	**394**	–	**395**	–	–
377(w)	–	–	**375**	–	**377**	–	–
373(w)	–	–	–	–	–	–	–
340(w)	**340**	–	**337**	–	**339**	–	–
328(vw)	–	–	–	–	–	–	–
302(vw)	–	–	–	–	–	–	–
298(vw)	–	–	**296**	–	**295**	–	–
294(vw)	–	–	–	–	–	–	–
273(vw)	–	–	–	–	**272**	–	–
262(vw)	–	–	**265**	–	**266**	–	–
252(vw)	–	–	–	–	–	–	–
185(vw)	–	–	–	–	–	–	–
148(vw)	–	–	–	–	**145**	–	–
141(vw)	–	–	**140(?)**	–	–	–	–
105(vw)	–	–	–	–	–	–	–

[a] W2013, Wehinger et al. (2013; theoretic calculation); L1958, Lippincott et al. (1958; synthetic Coe powder + KBr); L1962, Lyon (1962; natural Coe powder + KBr); K1979, Kieffer (1979a; natural Coe powder + KBr); W1993, Williams et al. (1993; synthetic Coe powder + CsI); K2013, Koike et al. (2013; synthetic Coe powder + KBr); TS1, This study (~5-μm-thick Coe crystal plate with unknown crystallographic orientation); TS2, This study (~19-μm-thick Coe crystal plate with unknown crystallographic orientation). All experimental IR data were collected with unpolarized light.

[b] w, weak peak; vw, very weak peak; s, strong peak; vs very strong peak.

[c] Peak unobserved.

observed for Coe, much less than the 36 predicted A_u and B_u modes (Table 1).

Several experimental studies have been conducted to constrain the IR features of Coe with a Coe powder (pure synthetic sample or natural sample admixed with minor impurities) + KBr (or CsI) method (Lippincott et al., 1958; Lyon, 1962; Kieffer, 1979a; Williams et al., 1993; Koike et al., 2013; Table 1). Theoretically, both Dowty (1987) and Wehinger et al. (2013) probed the lattice dynamics of Coe and explored its IR characteristics. Della Valle and Andersen (1991) also calculated the lattice vibrations of Coe, with the main purpose of using their derived IR and Raman properties to test a pairwise additive ionic potential model for silica; unfortunately, the full and correct IR features of Coe were not available at that time.

The present study provides the first IR absorbance data collected on single crystals of Coe, removes many uncertainties in the peak positions and peak intensities inherited from the powder IR spectra (Beran et al., 2004), and thus sheds important lights on the lattice dynamics of this geologically important mineral.

As shown in Fig. 2, the most prominent IR peaks nominally occurred

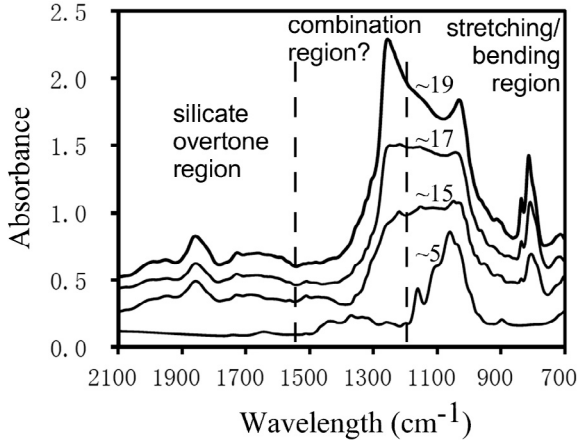

Fig. 2. Typical unpolarized IR absorbance spectra of Coe single crystals (with undetermined crystallographic orientations). The bright and clear portion of the analyzed Coe crystal plates was usually ~50 × 50 μm^2. The thicknesses of these particular crystal plates from which the shown IR spectra were collected were estimated as ~19, 17, 15 and 5 μm (from the top spectrum to the bottom spectrum). Other analytical conditions applied to the background and the sample analyses were 20 × 20 μm^2 beam size, 8 cm^{-1} resolution and 512 scans. Note the error in the top three spectra: the data in the ~1300–1000 cm^{-1} range are artifacts caused by too strong absorption.

in the range of ~1300–1000 cm^{-1}, in general agreement with all earlier experimental investigations (Lippincott et al., 1958; Lyon, 1962; Kieffer, 1979a; Williams et al., 1993; Koike et al., 2013). However, the transmitted light in this energy region was close to 0%, 8(2)% and 15(2)% for the crystal plate with the thickness of ~19, 17 and 15 μm, respectively. Consequently, these three IR spectra could not reveal the true IR features. As the crystal thickness was reduced to ~5 μm, indeed, the real and distinctly different IR peaks emerged in the range of ~1200–1000 cm^{-1}, which essentially agreed with the result of the normal coordinate calculation performed by Dowty (1987). Equally, the IR features at ~1830 and 795 cm^{-1} in the IR spectra collected from the thicker crystals lost their signals in the IR spectrum from the ~5-μm-thick crystal.

As a result, we can tentatively divide the IR spectra shown in Fig. 2 into three regions: the ~2100–1550 cm^{-1} region is the silicate overtone region, the ~1550–1200 cm^{-1} region is presumably a combination region, and the rest region is mostly the stretching/bending region of the SiO_4 tetrahedron. The energy range of the second order silicate overtones of Coe is much comparable to that of olivine which contains isolated SiO_4 tetrahedra, ~2100–1600 cm^{-1} (Jamtveit et al., 2001; Wang et al., 2015). Although the second order silicate overtones of Coe are weak and diffusive, they may be used to determine the crystallographic orientation and constrain the anharmonicity of the lattice dynamics (Jamtveit et al., 2001; Asimow et al., 2006; Wang et al., 2015). The IR peaks in the ~1550–1200 cm^{-1} region are generally stronger than the second order silicate overtones, and highly possibly originate from the interaction of the SiO_4 stretching/bending vibration modes and the most intense Raman band at ~521 cm^{-1} (e.g. Boyer et al., 1985; Liu et al., 1997). Alternative explanation such as the interaction of the SiO_4 stretching/bending vibration modes with the less intense Raman/IR bands in the energy range less than 500 cm^{-1} is less likely; interaction of this kind would lead to much lower intensities for the peaks in the ~1550–1200 cm^{-1} region than for those in the ~2100–1550 cm^{-1} region, right opposite to what we observed (Fig. 2).

To accurately constrain the positions of the most intense IR bands, the IR spectrum taken on the ~5-μm-thick crystal has been carefully deconvoluted (Fig. 3). In total five sharp and strong peaks are resolved at ~1161, 1109, 1063, 1028 and 994 cm^{-1}, with two less intense peaks occurring at ~1199 and 965 cm^{-1}. Previously only four IR peaks were constantly observed at ~1225, 1170, 1098 and 1040 cm^{-1} for the energy range of ~1250–950 cm^{-1} (Lippincott et al., 1958; Lyon, 1962;

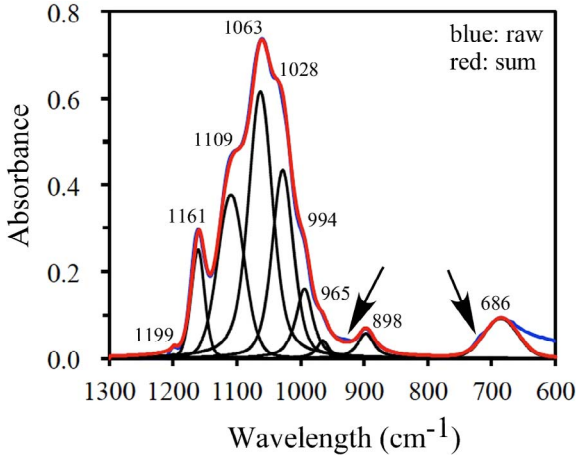

Fig. 3. Gaussian-Lorentzian deconvolution of the IR absorbance spectrum taken on the ~5-μm-thick Coe crystal plate (the 1300–600 cm^{-1} region). We used the PeakFit V4.12 software (SPSS Inc.) to process the IR data. The sum (the red curve) of the nine Gaussian-Lorentzian peaks (the black curves) agrees well with the raw data (the blue curve without baseline correction) for the most data range. The exceptions are two possible very weak peaks at ~940 and 720 cm^{-1} (as indicated by the two black arrows) which did not fully show up due to the very thin sample employed in collecting this spectrum (positively confirmed by the IR data collected on a thicker sample; Fig. 4 and Table 1), and the apparent difference between the sum and the raw at the low energy side of the peak ~686 cm^{-1} which is believed as an experimental artifact caused by our IR experimental setting-up.

Kieffer, 1979a; Williams et al., 1993; Table 1). On the base of our new IR data, we are confident that (1) the previously observed band at ~1225 cm^{-1} has very low intensity and is mostly a combination mode, (2) although poorly resolved due to the employed experimental method (powder IR spectrum), the previously observed bands at ~1170, 1098 and 1040 cm^{-1} are generally comparable to the peaks at ~1161, 1109 and 1028 cm^{-1} observed in this study, and (3) the most intense bands expected to associate with the SiO_4 asymmetric stretch (ν_3) occur in the energy range of ~1161–994 cm^{-1}, but their precise assignment must await further polarized single-crystal IR absorption and reflectance data.

The origin of the sharp bands at ~838, 814 and 796 cm^{-1} is less certain (Fig. 4). These peaks are either the SiO_4 symmetric stretching modes (ν_1) or the SiO_4 asymmetric bending modes (ν_4), considering the order in the energies of the SiO_4 vibration modes ($\nu_3 > \nu_1 > \nu_4 > \nu_2$,

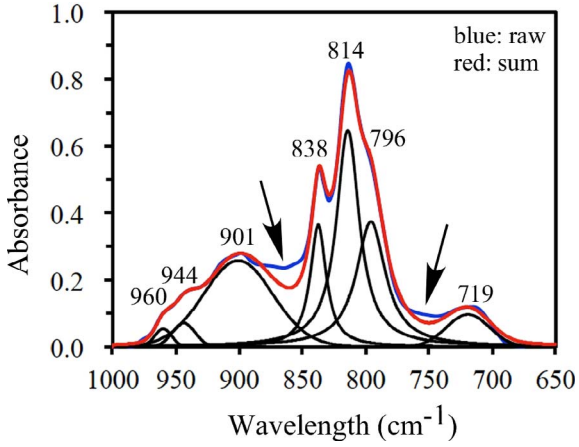

Fig. 4. Gaussian-Lorentzian deconvolution of the IR absorbance spectrum taken on the ~19-μm-thick Coe crystal (the 1000–650 cm^{-1} region). The sum (the red curve) of the seven Gaussian-Lorentzian peaks (the black curves) agrees well with the raw data (the blue curve without baseline correction) for the most data range. The exceptions are possible very weak and diffusive peaks at ~870 and 750 cm^{-1} (as indicated by the two black arrows) which did not clearly show up mostly due to inappropriate crystallographic orientation.

with ν_2 representing the SiO_4 symmetric bending modes; Nakamoto, 1978). If the former were correct, the positions of the ν_1 modes of the SiO_4 tetrahedra would agree with those of the ν_1 modes of the SiO_4 tetrahedra in forsterite (~840.8 and 828 cm^{-1}; Hofmeister, 1987). However, the ν_1 mode of the SiO_4 tetrahedra is nondegenerate and IR-inactive under normal circumstance (Beran et al., 2004). The latter is thus our preferred assignment: the ν_4 mode of the SiO_4 tetrahedra is triply degenerate and IR-active, although the positions of the observed bands are at much higher energies than those usually attributed to the SiO_4 bending modes (550–400 cm^{-1}; Beran et al., 2004). This is possible. Let us compare the SiO_4 tetrahedra in Coe and in forsterite: Coe is a framework silicate with corner-sharing SiO_4 tetrahedra whereas forsterite is an orthosilicate with completely isolated SiO_4 tetrahedra, so that the Si-O bonds in Coe are expected to be stronger than those in forsterite. Indeed, the ν_3 modes of the SiO_4 tetrahedra in Coe occur at relatively higher energies (~1161–994 cm^{-1}), compared to those in forsterite (~988–865 cm^{-1}; Hofmeister, 1987). Following the same principle, the ν_4 modes of the SiO_4 tetrahedra in Coe may appear at higher energies as well.

Other IR peaks shown in Fig. 3 (at 1199, 965, 898 and 686 cm^{-1}) or in Fig. 4 (at 960, 944, 901 and 719 cm^{-1}) have low intensities and are diffusive, so that they do not represent normal IR modes but combination bands or overtones.

For the IR features of Coe at lower wavenumbers than ~612 cm^{-1}, good agreement has been established among those earlier experimental studies (Table 1). The experimental results appear compatible to the simulating results as well. On the other hand, a large number of the IR peaks in this energy range predicted by the simulation has not been experimentally observed, which requires further experimental investigation.

Coe is one of the SiO_2 polymorphs (such as α- and β-quartz, α- and β-cristobalite, and Coe; Heaney, 1994) which display different density, different symmetry, and different medium- and long-range arrangement of the SiO_4 tetrahedra. Understanding their vibrational dynamics does not only provide the knowledge about the mechanical, elastic and thermodynamic properties for these minerals, but also deepen our understanding of other silicate minerals and melts. IR is one of the mostly-employed tools to probe the vibrational dynamics of a material. Since Coe has the highest density among the polymorphs mentioned above, its IR data with high accuracy is very important. Our IR data have been collected on single crystals of Coe, and eliminated many flaws in the previous IR spectra taken with the powder method; in particular, the IR features for the SiO_4 asymmetric stretching modes determined in this study are very different to the experimental results in the literatures, and so are the IR features of the SiO_4 asymmetric bending modes. On the basis of the present study, we tend to believe that all the old IR data of the SiO_2 polymorphs collected with the powder method may be subject to similar problems, so that some careful revision appears necessary. Only with the new data of high accuracy may we possibly resolve the discrepancies existing between the old experimental IR data and the simulated IR features (Dowty, 1987; Della Valle and Andersen, 1991; Wehinger et al., 2013).

3.2. IR features of OH in Coe

Coe is nominally anhydrous, and natural Coe (except the Coe inclusion in one of the diamonds from Venezuela; Koch-Müller et al., 2003) is usually found as water-free (Rossman and Smyth, 1990; Mosenfelder et al., 2005). However, a large number of high-*P* experimental studies have suggested that Coe can contain some structurally-bounded water (Table 2; Mosenfelder, 2000; Koch-Müller et al., 2001, 2003; Lathe et al., 2005; Deon et al., 2009; Thomas et al., 2009). With unpolarized single-crystal FTIR spectra, Mosenfelder (2000) observed sharp water peaks in synthetic Coe at ~3606, 3573, 3523, 3459 and 3299 cm^{-1}, as previously observed by Li et al. (1997). Using similar experimental techniques, Koch-Müller et al. (2001) did not observe the

Table 2
IR frequencies (cm^{-1}) of OH peaks in Coe observed with unpolarized IR spectra collected at ambient *P-T* conditions.

M2000	KM2001	KM2003	D2009	T2009	This Study
1200[a]	1100[a]	750–1300[a]	1022–2000[a]	930–1400[a]	1600[a]
5–10[b]	6.5–7.5[b]	6.5–9[b]	9.1–11.9[b]	7.5–9.1[b]	5[b]
3606	–	–	–	–	–
3573	3575(#1)	3575(#1)	–	3576(#1)	–
–	–	3535(#6b)	3535(#6b)	3535(#6b)	3534(#6b)
–	–	–	3520(#6c)[c]	–	–
3523	3516(#2)	3516(#2)	–	3520(#2)	–
–	(3528(#2a))	(3528(#2a))	–	–	–
–	(3508(#2b))	(3508(#2b))	–	–	–
–	–	3502(#6a)	3500(#6a)	3500(#6a)	3500(#6a)
–	–	3460(#7)	3460(#7)	3460(#7)	3464(#7)
3459	3459(#3)	3459(#3)	–	3459(#3)	–
–	–	3422(#8)	3422(#8)	3422(#8)	3421(#8)
–	–	3407(#9)	3407(#9)	3407(#9)	3406(#9)
–	–	3379(#10)	3379(#10)	3379(#10)	3377(#10)
3299	3296(#4)	3300(#4)	–	3300(#4)	–
–	3210(#5)	3210(#5)	–	3210(#5)	–

M2000, Mosenfelder et al. (2000); KM2001, Koch-Müller et al. (2001); KM2003, Koch-Müller et al. (2003); D2009, Deon et al. (2009); T2009, Thomas et al. (2009).
[a] *T* in °C for synthesizing experiments.
[b] *P* in GPa for synthesizing experiments.
[c] Position determined at −100 °C.

weak water peak at ~3606 cm^{-1}, but confirmed the presence of other peaks, and found one extra peak at ~3210 cm^{-1} (#5; Table 2). Further, they revealed that the peak at ~3516 cm^{-1} (#2) was strongly asymmetric and had two components (#2a at ~3528 and #2b at ~3508 cm^{-1}), and demonstrated that the peaks #1 (~3575 cm^{-1}), #2 (#2a and #2b) and #3 (~3459 cm^{-1}) were due to the Type-I hydrogarnet substitution ($Si^{4+(Si2)} + 4O^{2-} = {}^{[4]}\square^{(Si2)} + 4OH^-$), and the peaks #4 (~3296 cm^{-1}) and #5 were due to the Al-based defects ($Si^{4+} = Al^{3+} + H^+$). Additionally, Koch-Müller et al. (2003) observed some more water peaks at ~3460 (#7), 3422 (#8), 3407 (#9) and 3379 cm^{-1} (#10) which they attributed to the Type-II hydrogarnet substitution ($Si^{4+(Si1)} + 4O^{2-} = {}^{[4]}\square^{(Si1)} + 4OH^-$), and at ~3502 (#6a) and 3535 cm^{-1} (#6b) which they attributed to the B-based defects ($Si^{4+} = B^{3+} + H^+$). These experimental results were generally confirmed by later investigations (Deon et al., 2009; Thomas et al., 2009; Table 2).

In our synthesizing experiments, water was not introduced deliberately. But some hydrogen, as generated by contaminant moisture reacting with the graphite heater, would diffuse through the Pt capsule, react with the experimental charge and generate some water (Liu and O'Neill, 2004a, 2004b), which would subsequently enter the Coe structure. Indeed, six water peaks were found for our Coe at ~3534, 3500, 3464, 3421, 3406 and 3377 cm^{-1} (Fig. 5 and Table 2). On the basis of the Coe-specific calibration established by Koch-Müller et al. (2001), the H_2O content in the Coe was estimated as 30(4) wt ppm by applying the Beer-Lambert law (six unpolarized IR spectra collected from randomly-selected single crystals; see later discussion). This water content is slightly lower than the water solubility in Coe at 5 GPa and 1200 °C (~43 wt ppm, a value potentially overestimated; Mosenfelder, 2000; Koch-Müller et al., 2001, 2003). If the water solubility in Coe at certain *P* positively correlates with *T* as found in Koch-Müller et al. (2001, 2003), a free fluid phase would not have been present in our high-*P* synthesizing experiments; otherwise, a higher water content should have been observed for our Coe. If the water solubility negatively correlates with *T* as found in Deon et al. (2009), on the other hand, our Coe would have been in equilibrium with a trace amount of fluid/melt which would have had less amounts of water as *T* increased to our experimental *T* (1600 °C), a result in agreement with the phase relations in the system SiO_2-H_2O (Kennedy et al., 1962; Liu et al., 2009).

All the water peaks observed in this study were experimentally

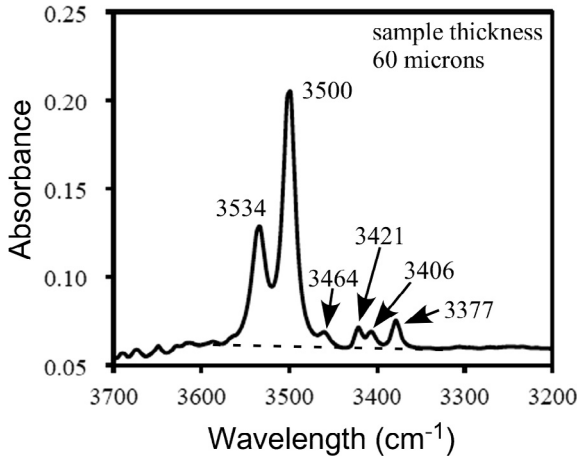

Fig. 5. Typical unpolarized IR absorbance spectrum of Coe single crystal (with undetermined crystallographic orientation) and the water peaks. The crystal plate had a thickness of ~60 μm. Other analytical conditions applied to the background and the sample analyses were 30 × 30 μm^2 beam size, 8 cm^{-1} resolution and 256 scans. To quantify the water content, the background correction was made by drawing a straight line in the energy region ~3600–3300 cm^{-1} (the dashed line), and the areas under the six water peaks were summed to generate the total integrated absorbance. The water content was eventually calculated by using the Beer-Lambert law, with the Coe-specific integrated molar absorption coefficient from Koch-Müller et al. (2001). The density of the Coe was assumed as ideal.

demonstrated before (Koch-Müller et al., 2001, 2003; Deon et al., 2009; Thomas et al., 2009; Table 2). According to these studies, we can assign the peaks at ~3464 (#7), 3421 (#8), 3406 (#9) and 3377 cm^{-1} (#10) to the Type-II hydrogarnet substitution ($Si^{4+(Si1)} + 4O^{2-} = {}^{[4]}\square^{(Si1)} + 4OH^-$), and the peaks at ~3500 (#6a) and 3534 cm^{-1} (#6b) to the B-based defects ($Si^{4+} = B^{3+} + H^+$). Some boron contamination in our high-*P* synthesizing experiments was possible (Liu and O'Neill, 2004a) since small parts made from *h*BN material were employed in the cell arrangement BJC-11 (He et al., 2014) and routinely used in the High-Pressure Laboratory of Peking University (Liu et al., 2012). Further, the ratio of the peak heights of #6a (~3500 cm^{-1}) and #10 (3377 cm^{-1}) is ~11(3), much smaller than that observed in Deon et al. (2009; Fig. 2) and Thomas et al. (2009; Fig. 3). It follows that the B-based defects had a smaller role in incorporating water into our Coe whereas the Type-II hydrogarnet substitution mechanism made a larger contribution, compared to the cases in Deon et al. (2009) and Thomas et al. (2009).

It is interesting to note that no obvious IR peaks have been observed in this study at ~3575 (#1), 3516 (#2) and ~3459 cm^{-1} (#3), and at ~3296 (#4) and 3210 cm^{-1} (#5) (Table 2). As discussed before, the peaks of the former group were attributed to the Type-I hydrogarnet substitution ($Si^{4+(Si2)} + 4O^{2-} = {}^{[4]}\square^{(Si2)} + 4OH^-$), and the peaks of the latter group were due to the Al-based defects ($Si^{4+} = Al^{3+} + H^+$). No Al was introduced into our starting material used in the high-*P* synthesizing experiments, and no #4 and no #5 should be expected. Koch-Müller et al. (2003) suggested that high pressure might suppress the peaks #1, #2 and #3. Our synthesizing experiments and the Run 886 reported by Mosenfelder (2000) were conducted at the same *P* (5 GPa), but with other different experimental details (such as 1600 vs 1200 °C, no fo_2 buffer vs Ni-NiO buffer, no coexisting phase vs Ni-rich pyroxene and (Ni, Mg)$_2SiO_4$-spinel in equilibrium). This means that other factors, including high *T* and some compositional variables, may be able to suppress the Type-I hydrogarnet substitution in Coe as well.

3.3. Amorphization of Coe

Coe is a thermodynamically metastable phase at ambient *P*, with a thermodynamic melting temperature (T_m) of ~602 °C (Richet, 1988). For the pure SiO_2 system, the standard glass transition temperature (T_g) is 1207 °C (Richet et al., 1982). At *T* between the T_m and T_g, Coe

becomes amorphous via a heterogeneous nucleation-and-growth controlled process in which amorphous domains nucleate at free surfaces and grain boundaries, and the amorphous-crystalline interface propagates into the interior of the crystals (Gong et al., 1996). This amorphization process is slow, and time- and *T*-dependent. As demonstrated by Gong et al. (1996), the amorphous layer is only ~25 nm thick for an annealing time of 1.5 h, and ~60 nm thick for an annealing time of 3.5 h at 927 °C. Indeed, regular high-*T* Raman spectroscopic experiments up to ~1127 °C did not show any clear signal of amorphization (Gillet et al., 1990; Liu et al., 1997), and common high-*T* X-ray diffraction measurements up to T_g (1207 °C) did not reveal obvious amorphization as well (Skinner, 1962; Bourova et al., 2006), presumably due to the relatively short heating time between the T_m and T_g.

Prolonged annealing experiments were conducted by Dachille et al. (1963), Gillet et al. (1990), Brazhkin et al. (1991) and Gong et al. (1996), and different phase transition schemes were obtained. Dachille et al. (1963) conducted extensive annealing experiments on Coe, and suggested that Coe probably experienced some amorphization for an annealing time of 550 h at 1070 °C, but from ~1100 °C to the T_g it transformed to quartz which in turn transformed to cristobalite (the stable form of SiO_2 from 1470 to 1727 °C; Heaney, 1994), with intermediate amorphous forms preceding the emergence of each crystal modification. Gillet et al. (1990) observed a direct phase transition from Coe to cristobalite at ~1087 °C. Brazhkin et al. (1991) demonstrated a phase-transition scheme of Coe → amorphous form → cristobalite at ~1107–1147 °C. Gong et al. (1996) discovered a very slow phase transition from Coe to an amorphous form at ~927 °C.

The results of our annealing experiments are shown in Figs. 6 and 7. Annealing the Coe thin section (~60 μm thick) consecutively at ~200, 400, 600, 800 and 1000 °C for 24 h at every step did not produce much amorphization, as indicated by the constant positions of the IR peaks. Using the data in Gong et al. (1996) and making a linear extrapolation, annealing Coe at ~927 °C for 24 h would have produced a ~0.4-μm-thick amorphous layer on each side of the Coe crystals. The total thickness of the amorphous layers formed in our annealing experiments up to 1000 °C then would be in the range of ~2 μm only, so that their IR signal would be relatively weak and totally concealed by the much stronger IR signal of the voluminous Coe (~58 μm thick). Amorphization process may speed up at higher *T*. After further annealing at 1200 °C for 24 h, a complete amorphous state was achieved (Figs. 6 and 7). Fig. 6 shows that the peaks of the fundamental ν_4 modes of the SiO_4 tetrahedra in Coe have disappeared completely, and a much broader new peak has occurred at slightly higher wavenumbers. The position of this new IR peak seemingly agrees only with one of the IR features of the vitreous SiO_2 (Lippincott et al., 1958) or fused quartz (Koike et al., 2013). The IR features in the silicate overtone region show many drastic changes (Fig. 7): six Coe peaks (a, b, c, d, e, and g) have disappeared whereas five new peaks (I, II, III, IV, and V) have occurred in the IR spectra collected on the crystals annealed at 1200 °C. The broad and smooth nature of these new IR peaks implies that the material is completely amorphous. Our annealing experiments thus have suggested that at 1200 °C Coe transforms to an amorphous form before any further phase transition (if there is any) takes place, in agreement with Dachille et al. (1963), Brazhkin et al. (1991) and Gong et al. (1996).

The drastic changes of the IR features in the silicate overtone region accompanying the phase transition observed here imply that the IR features in the silicate overtone region are potentially very useful. To achieve good signal for the fundamental vibration modes of the SiO_4 tetrahedra, a very thin sample is usually required, but hard to prepare. On the other hand, good signal for the lattice vibration modes can be acquired from relatively thick sample with appropriate IR detector, which is usually not equipped though.

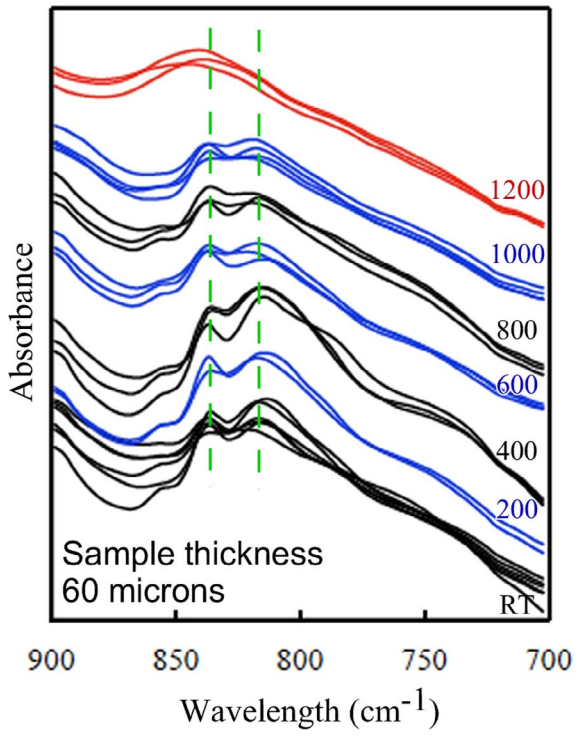

Fig. 6. Unpolarized IR absorbance spectra (900–700 cm^{-1}) collected on single crystals (with undetermined crystallographic orientations) annealed at different *T*. Analytical conditions were identical to those applied to the spectrum shown in Fig. 5. The two major peaks (as denoted by the green broken lines) can be traced at least up to 1000 °C.

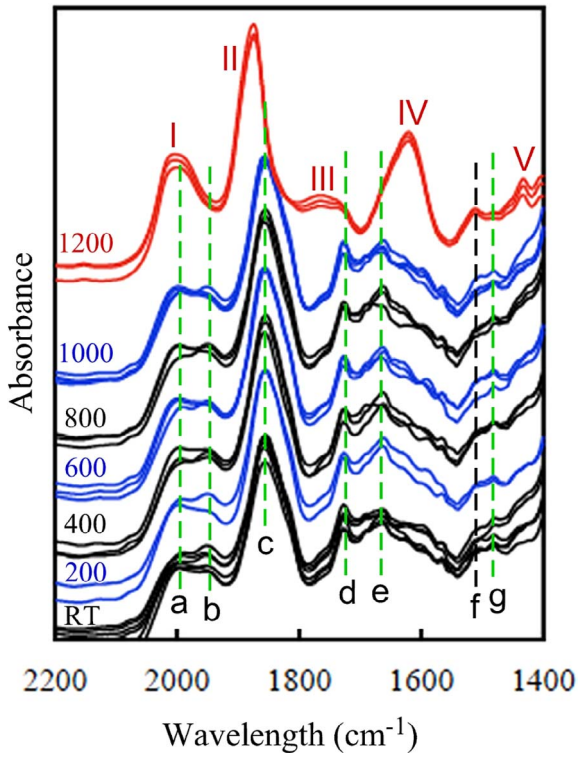

Fig. 7. Unpolarized IR absorbance spectra (2200–1400 cm^{-1}) collected on single crystals (with undetermined crystallographic orientations) annealed at different *T*. Analytical conditions were identical to those applied to the spectrum shown in Fig. 5. Some peaks (a, b, c, d, e and g, as denoted by the green broken lines) can be traced at least up to 1000 °C, but disappear at 1200 °C. A few peaks, taking peak f as one example (denoted by the black broken line), remain discernable at 1200 °C. The material annealed at 1200 °C has attained some new IR peaks (I, II, III, IV, and V).

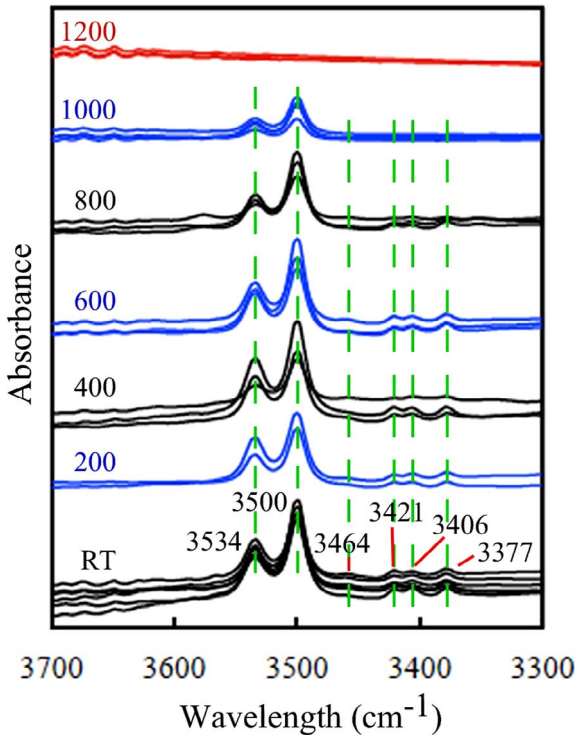

Fig. 8. Unpolarized IR absorbance spectra (3700–3300 cm^{-1}) collected on single crystals (with undetermined crystallographic orientations) annealed at different *T*. Analytical conditions were identical to those applied to the spectrum shown in Fig. 5.

3.4. Dehydration of Coe

The IR spectra in the range of 3700–3300 cm^{-1} collected on our Coe sample consecutively annealed at different *T* are shown in Fig. 8. The six room-*T* spectra obtained from randomly selected Coe grains are very similar, and thus suggest a weak pleochroic behavior for these water peaks, in good agreement with Deon et al. (2009; Fig. 3a). For the whole annealing process, no new water peak was observed. As the annealing *T* increased from room *T* to at least up to 1000 °C, all the water peaks could be confidently traced, with the peaks at ~3464, 3421, 3406 and 3377 cm^{-1} in the spectra collected from the sample annealed at 1000 °C being discernibly weak though. In contrast, all these peaks disappeared from the IR spectra collected from the material annealed at 1200 °C, indicating a complete dehydration.

The water contents are shown in Fig. 9. With the present annealing conditions, the Coe grains started to lose water at ~600 °C (27(5) wt ppm left), lost about one third of the water at ~800 °C (22(6) wt ppm left), and lost about two thirds of the water at 1000 °C (9(2) wt ppm left). As discussed before, the incorporation of water in our Coe could be due to the B-based defects (peaks #6a and #6b) and the Type-II hydrogarnet substitution (peaks #7, #8, #9 and #10). Within the resolution of our data, these two kinds of water had similar behavior in the dehydration process: they were lost at similar rates, and there was little exchanging between them. It should be interesting to check if other types of water in Coe (such as the water species due to the Al-based defects and the Type-I hydrogarnet substitution) behave similarly in the dehydration process.

There has not been any specifically-designed experimental investigation on the diffusion process of water in Coe. Our annealing experiments at ambient *P* did not produce any quantitative data, but generally showed that the Coe lost ~10 wt% of its water by annealing at 600 °C for 24 h. It is thus clear that water may be quickly lost from Coe at much lower *T*. At high *P* and *T* conditions, Coe-synthesizing experiments conducted at 5–10 GPa and 1200 °C for 12 h produced large crystals (up to ~200 μm) with homogeneous water distribution

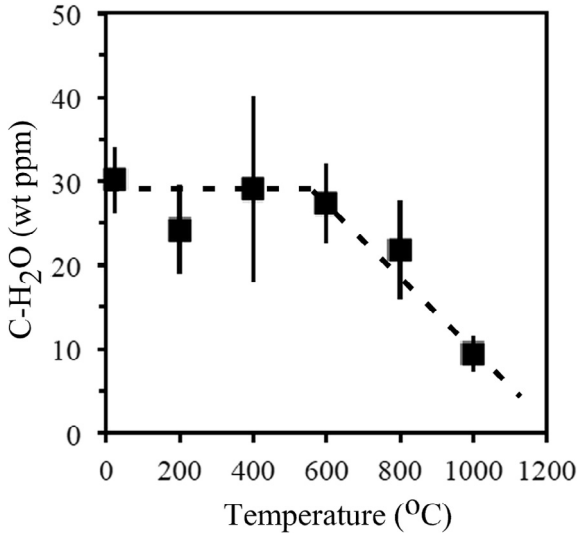

Fig. 9. Evolution of average water content in single crystals annealed at different *T*. The original IR spectra from which these water contents were derived are shown in Fig. 8.

(Mosenfelder, 2000). Koch-Müller et al. (2001) performed a two-step synthesizing experiment (MKM-00-15), with the experiment firstly conducted in the quartz stability field (1.5 GPa and 600 °C) for 14 h and secondly run in the Coe stability field (7.5 GPa and 1100 °C) for 27 h to equilibrate the water content, in which homogeneous Coe crystals up to several hundred microns were formed. We are thus intrigued to propose that water diffusion in Coe may be very fast at typical *P-T* conditions in normal mantle and subduction zone.

A fast water diffusion rate in Coe helps resolving the nominal conflict between the high-*P* experimental results and the field observations: water-rich synthetic Coe vs water-poor natural Coe (Rossman and Smyth, 1990; Li et al., 1997; Mosenfelder, 2000; Koch-Müller et al., 2001, 2003; Mosenfelder et al., 2005). As experimentally suggested, the water solubility in Coe positively correlates with *P* (Mosenfelder, 2000), and arguably with *T* as well (Koch-Müller et al., 2003; Deon et al., 2009), so that the water solubility in Coe subject to continues cooling during decompression should be almost zero when the *P-T* conditions come close to those of the phase transition Coe = quartz. A fast water diffusion rate should secure a timely response of the water content in Coe to the changes of *P*, *T*, and composition, facilitating the partial preservation of Coe in the end (Mosenfelder and Bohlen, 1997; Lathe et al., 2005). On the other hand, significant water in Coe may be retained only if Coe is fully included in water-free minerals such as diamond and completely isolated from the surroundings (Koch-Müller et al., 2003).

Coe is one of the nominally anhydrous minerals (NAMs) in the subducted continental crustal material which contain trace amounts of water in their structures (Johnson, 2006); other NAMs include quartz, omphacite, garnet, kyanite, rutile, zircon, and etc. The variations of the water-incorporation mechanism, the water solubility, and the water diffusion rate in these minerals in response to changes in *P*, *T* and composition are presently largely unknown. Nevertheless, our preliminary results on the dehydration process of Coe, plus other evidences (Mosenfelder, 2000; Koch-Müller et al., 2001), suggest that water may readily enter or leave Coe when the water solubility changes. If this is also the case for the water in other NAMs, the dissolved water may have important influence on the geochemical, geophysical and geodynamic evolution of the subducted crustal material, considering the much larger volume proportion of the NAMs compared to that of the hydrous phases such as amphibole and mica. When the subducted crustal material experiences its exhumation, decreasing *P* results in gradually lower water solubilities in the NAMs, and quick water diffusion rates imply significant and inevitable water release, which may indeed have

triggered the partial melting process during continental collision, as frequently recorded by the ultrahigh-pressure metamorphic rocks (Zheng et al., 2011).

In contrast, the water locked in the hydrous phases may make much less significant contribution. Firstly, the proportion of the hydrous phases is usually much lower. Secondly, the release of water from the hydrous phases is much dependent on the breakdown reactions which may be kinetically sluggish at relatively low *T*. Thirdly, the instability field of the hydrous phases may be substantially reduced by the water released from the NAMs.

4. Conclusions

Our unpolarized single-crystal absorption FTIR investigation on Coe suggests the following points:

(1) The SiO_4 asymmetric stretching (ν_3) of Coe locates in the energy range of ~1161–994 cm^{-1} (presumably five peaks at ~1161, 1109, 1063, 1028 and 994 cm^{-1}) whereas the SiO_4 asymmetric bending (ν_4) perhaps appears at ~838, 814 and 796 cm^{-1}.
(2) Six OH peaks occur in the range of 3700–3300 cm^{-1} for our synthetic Coe. The peaks at ~3464 (#7), 3421 (#8), 3406 (#9) and 3377 cm^{-1} (#10) can be attributed to the Type-II hydrogarnet substitution, and the peaks at ~3500 (#6a) and 3534 cm^{-1} (#6b) to the B-based defects (Table 2).
(3) Water quickly diffuses out of Coe at *T* as low as 600 °C (Fig. 9). A quick response of the water content to the changes of *P*, *T* and composition is thus evident, and may facilitate the preservation of natural Coe in relevant geological processes.
(4) Water in Coe, and possibly in other NAMs, may behave very differently to the water locked in the hydrous phases. Water in the NAMs may be readily released and cause partial melting as the subducted continental crustal material exhumes.

Acknowledgements

We thank three anonymous reviewers for their constructive and insightful comments, and Prof. Yongfei Zheng for his editorial handling of this paper. This study was financially supported by the Strategic Priority Research Program (B) of Chinese Academy of Sciences (Grant No. XDB18000000), by the DREAM project of MOST, China (Grant No. 2016YFC0600408), and by the Program of the Data Integration and Standardization in the Geological Science and Technology from MOST, China (Grant No. 2013FY110900-3).

References

Akaogi, M., Yusa, H., Shiraishi, K., Suzuki, T., 1995. Thermodynamic properties of α-quartz, coesite, and stishovite and equilibrium phase relations at high pressures and high temperatures. J. Geophys. Res. 100, 22337–22347.
Angel, R.J., Mosenfelder, J.L., Shaw, C.S.J., 2001. Anomalous compression and equation of state of coesite. Phys. Earth Planet. Inter. 124, 71–79.
Angel, R.J., Shaw, C.S.J., Gibbs, G.V., 2003. Compression mechanisms of coesite. Phys. Chem. Mineral. 30, 167–176.
Araki, T., Zoltai, T., 1969. Refinement of a coesite structure. Z. Kristallogr. 129, 381–387.
Asimow, P.D., Stein, L.C., Mosenfelder, J.L., Rossman, G.R., 2006. Quantitative polarized infrared analysis of trace OH in populations of randomly oriented mineral grains. Am. Miner. 91, 278–284.
Atake, T., Inoue, N., Kawaji, H., Matsuzaka, K., Akaogi, M., 2000. Low-temperature heat capacity of the high-pressure-phase of SiO_2, coesite, and calculation of the α-quartz-to-coesite equilibrium boundary. J. Chem. Thermodyn. 32, 217–227.
Austin, I.G., Gebbie, H.A., Morin, I., 1961. Absorption of coesite in the wavelength region 5–22 microns. Proc. Phys. Soc. LXXVIII, 1260–1261.
Beran, A., Voll, D., Schneider, H., 2004. IR spectroscopy as a tool for the characterisation of ceramic precursor phases. EMU Notes Mineral. 6, 189–226.
Bourova, E., Richet, P., Petitet, J.-P., 2006. Coesite (SiO_2) as an extreme case of superheated crystal: an X-ray diffraction study up to 1776 K. Chem. Geol. 229, 57–63.
Boyer, H., Smith, D.C., Chopin, C., Lasnier, B., 1985. Raman microprobe (RMP) determinations of natural and synthetic coesite. Phys. Chem. Mineral. 12, 45–48.
Brazhkin, V.V., Voloshin, R.N., Popova, S.V., 1991. The kinetics of the transition of the metastable phases of SiO_2, stishovite and coesite to the amorphous state. J. Non-Cryst. Solids 136, 241–248.
Černok, A., Boffa Ballaran, T., Caracas, R., Miyajima, N., Bykova, E., Prakapenka, V., Liermann, H.P., Dubrovinsky, L., 2014. Pressure-induced phase transitions in coesite. Am. Miner. 99, 755–763.
Chao, E.C.T., Shoemaker, E.M., Madsen, B.M., 1960. First natural occurrence of coesite. Science 132, 220–222.
Chen, T., Gwanmesia, G.D., Wang, X., Zou, Y., Liebermann, R.C., Michaut, C., Li, B., 2015. Anomalous elastic properties of coesite at high pressure and implications for the upper mantle X-discontinuity. Earth Planet. Sci. Lett. 412, 42–51.
Chen, T., Wang, X., Qi, X., Ma, M., Xu, Z., Li, B., 2016. Elasticity and phase transformation at high pressure in coesite from experiments and first-principles calculations. Am. Miner. 101, 1190–1196.
Chopin, C., 1984. Coesite and pure pyrope in high-grade blueschists of the Western Alps: a first record and some consequences. Contrib. Mineral. Petrol. 86, 107–118.
Coes, L., 1953. A new dense crystalline silica. Science 118, 131–132.
Dachille, F., Zeto, R.J., Roy, R., 1963. Coesite and stishovite: stepwise reversal transformations. Science 140, 991–993.
Della Valle, R.G., Andersen, H.C., 1991. Test of a pairwise additive ionic potential model for silica. J. Chem. Phys. 94, 5056–5060.
Deon, F., Koch-Müller, M., Hövelmann, J., Rhede, D., Thomas, S.-M., 2009. Coupled boron and hydrogen incorporation in coesite. Eur. J. Mineral. 21, 9–16.
Dowty, E., 1987. Vibrational interactions of tetrahedra in silicate glasses and crystals: II. Calculations on melilites, pyroxenes, silica polymorphs and feldspars. Phys. Chem. Mineral. 14, 122–138.
Geisinger, K.L., Spackman, M.A., Gibbs, G.V., 1987. Exploration of structure, electron density distribution, and bonding in coesite with Fourier and pseudoatom refinement methods using single-crystal X-ray diffraction data. J. Phys. Chem. 91, 3237–3244.
Gillet, P., Le Cléac'h, A., Madon, M., 1990. High-temperature Raman spectroscopy of SiO_2 and GeO_2 polymorphs: anharmonicity and thermodynamic properties at high-temperatures. J. Geophys. Res. 95, 21635–21655.
Gong, W.L., Wang, L.M., Ewing, R.C., Fei, Y., 1996. Surface and grain-boundary amorphization: thermodynamic melting of coesite below the glass transition temperature. Phys. Rev. B 53, 2155–2158.
Heaney, P.J., 1994. Structure and chemistry of the low-pressure silica polymorphs. Rev. Mineral. 29, 1–40.
He, Q., Tang, J., Wang, F., Liu, X., 2014. High temperature stable assembly designed for cubic press. Chin. J. High Pressure Phys. 28, 145–151.
Hemley, R.J., 1987. Pressure dependence of Raman spectra of SiO_2 polymorphs: α-quartz, coesite, and stishovite. Geophys. Monogr. Ser. 39, 347–359.
Hofmeister, A.M., 1987. Single-crystal absorption and reflection infrared spectroscopy of forsterite and fayalite. Phys. Chem. Mineral. 14, 499–513.
Jamtveit, B., Brooker, R., Brooks, K., Larsen, L.M., Pedersen, T., 2001. The water content of olivines from the North Atlantic Volcanic Province. Earth Planet. Sci. Lett. 186, 401–415.
Johnson, E.A., 2006. Water in nominally anhydrous crustal minerals: speciation, concentration, and geologic significance. Rev. Mineral. Geochem. 62, 117–154.
Kennedy, G.C., Wasserburg, G.J., Heard, H.C., Newton, R.C., 1962. The upper three-phase region in the system SiO_2-H_2O. Am. J. Sci. 260, 501–521.
Kieffer, S.W., 1979a. Thermodynamics and lattice vibrations of minerals: 2. Vibrational characteristics of silicates. Rev. Geophys. Space Phys. 17, 20–34.
Kieffer, S.W., 1979b. Thermodynamics and lattice vibrations of minerals: 3. Lattice dynamics and an approximation for minerals with application to simple substances and framework silicates. Rev. Geophys. Space Phys. 17, 35–59.
Koch-Müller, M., Fei, Y., Hauri, E., Liu, Z., 2001. Location and quantitative analysis of OH in coesite. Phys. Chem. Mineral. 28, 693–705.
Koch-Müller, M., Dera, P., Fei, Y., Reno, B., Sobolev, N., Hauri, E., Wysoczanski, R., 2003. OH^- in synthetic and natural coesite. Am. Miner. 88, 1436–1445.
Koike, C., Noguchi, R., Chihara, H., Suto, H., Ohtaka, O., Imai, Y., Matsumoto, T., Tsuchiyama, A., 2013. Infrared spectra of silica polymorphs and the conditions of their formation. Astrophys. J. 778, 60.
Lathe, C., Koch-Müller, M., Wirth, R., Van Westrenen, W., Mueller, H.-J., Schilling, F., Lauterjung, J., 2005. The influence of OH in coesite on the kinetics of the coesite-quartz phase transition. Am. Miner. 90, 36–43.
Levien, L., Prewitt, C.T., 1981. High-pressure crystal structure and compressibility of coesite. Am. Miner. 66, 324–333.
Lippincott, E.R., Van Valkenburg, A., Weir, C.E., Bunting, E.N., 1958. Infrared studies on polymorphs of silicon dioxide and germanium dioxide. J. Res. Nat. Bur. Stand. 61, 61–70.
Li, W., Lu, R., Yang, H., Prewitt, C.T., Fei, Y., 1997. Hydrogen in synthetic coesite crystals. EOS 78, 736.
Liu, L., Mernagh, T.P., Hibberson, W.O., 1997. Raman spectra of high-pressure polymorphs of SiO_2 at various temperatures. Phys. Chem. Mineral. 24, 396–402.
Liu, X., O'Neill, H.St.C., 2004a. Partial melting of spinel lherzolite in the system CaO-MgO-Al_2O_3-SiO_2 ± K_2O at 1.1 GPa. J. Petrol. 45, 1339–1368.
Liu, X., O'Neill, H.St.C., 2004b. The effect of Cr_2O_3 on the partial melting of spinel lherzolite in the system CaO-MgO-Al_2O_3-SiO_2-Cr_2O_3 at 1.1 GPa. J. Petrol. 45, 2261–2286.
Liu, X., O'Neill, H., St, C., Berry, A.J., 2006. The effects of small amounts of H_2O, CO_2 and Na_2O on the partial melting of spinel lherzolite in the system CaO-MgO-Al_2O_3-SiO_2 ± H_2O ± CO_2 ± Na_2O at 1.1 GPa. J. Petrol. 47, 409–434.
Liu, X., Zhang, L., Hack, A.C., Zheng, H., Hu, X., Chang, L., He, Q., 2009. Effect of water on the partial melting process of some silicate systems: important implication of the second critical endpoint. Acta Petrol. Sin. 25, 3407–3421.
Liu, X., Chen, J., Tang, J., He, Q., Li, S., Peng, F., He, D., Zhang, L., Fei, Y., 2012. A large volume cubic press with a pressure-generating capability up to about 10 GPa. High Pressure Res. 32, 239–254.

Lyon, R.J.P., 1962. Infra-red confirmation of 6-fold co-ordination of silicon in stishovite. Nature 196, 266–267.
Mosenfelder, J.L., 1997. Fluids, the preservation of coesite, and the exhumation of UHP metamorphic rocks. Terra Abstr. 9, 20–21.
Mosenfelder, J.L., Bohlen, S.R., 1997. Kinetics of the coesite to quartz transformation. Earth Planet. Sci. Lett. 153, 133–147.
Mosenfelder, J.L., 2000. Pressure dependence of hydroxyl solubility in coesite. Phys. Chem. Mineral. 27, 610–617.
Mosenfelder, J.L., Schertl, H.-P., Smyth, J.R., Liou, J.G., 2005. Factors in the preservation of coesite: the importance of fluid infiltration. Am. Miner. 90, 779–789.
Nakamoto, K., 1978. Infrared and Raman Spectra of Inorganic and Coordination Compounds. John Wiley and Sons, New York.
Richet, P., 1988. Superheating, melting and vitrification through decompression of high-pressure minerals. Nature 331, 56–58.
Richet, P., Bottinga, Y., Deniélou, L., Petitet, J.P., Téqui, C., 1982. Thermodynamic properties of quartz, cristobalite and amorphous SiO_2: drop calorimetry measurements between 1000 and 1800 K and a review from 0 to 2000 K. Geochim. Cosmochim. Acta 46, 2639–2658.
Rossman, G.R., Smyth, J.R., 1990. Hydroxyl contents of accessory minerals in mantle eclogites and related rocks. Am. Miner. 75, 775–780.
Skinner, B.J., 1962. Thermal expansion of ten minerals. U.S. Geol. Surv. Res. Prof. Pap. 450D, D109–D112.
Smyth, J.R., Smith, J.V., Artioli, G., Kvick, Å., 1987. Crystal structure of coesite, a high-pressure form of SiO_2, at 15 and 298 K from single-crystal Neutron and X-ray diffraction data: test of bonding models. J. Phys. Chem. 91, 988–992.
Tang, J., Liu, X., Xiong, Z., He, Q., Shieh, S.R., Wang, H., 2014. High temperature X-ray diffraction, DSC-TGA, polarized FTIR and high pressure Raman spectroscopy studies on euclase. Bull. Mineral. Petrol. Geochem. 33, 289–298.
Thomas, S.-M., Koch-Müller, M., Reichart, P., Rhede, D., Thomas, R., Wirth, R., Matsyuk, S., 2009. IR calibrations for water determination in olivine, r-GeO_2, and SiO_2 polymorphs. Phys. Chem. Mineral. 36, 489–509.
Wang, F., Liu, X., Zheng, H., Zhang, L., 2015. Anharmonic vibration of the SiO_4 tetrahedron in olivine at temperatures in the subduction zone: an infrared absorbance spectroscopic study. Acta Petrol. Sin. 31, 1891–1900.
Wehinger, B., Bosak, A., Chumakov, A., Mirone, A., Winkler, B., Dubrovinsky, L., Dubrovinskaia, N., Brazhkin, V., Dyuzheva, T., Krisch, M., 2013. Lattice dynamics of coesite. J. Phys.: Condens Matter 25, 275401–275408.
Williams, Q., Hemley, R.J., Kruger, M.B., Jeanloz, R., 1993. High-pressure infrared spectra of α-quartz, coesite, stishovite and silica glass. J. Geophys. Res. 98, 22157–22170.
Zheng, Y.-F., Xia, Q.-X., Chen, R.-X., Gao, X.-Y., 2011. Partial melting, fluid supercriticality and element mobility in ultrahigh-pressure metamorphic rocks during continental collision. Earth Sci. Rev. 107, 342–374.